GLUON RADIATION PATTERNS IN HADRONIC COLLISIONS *

D. ZEPPENFELD

Department of Physics, University of Wisconsin, 1150 University Ave.
Madison, WI 53706, USA
E-mail: dieter@phenom.physics.wisc.edu

(Received May 7, 1996)

The radiation pattern of soft gluons in hard scattering events is sensitive to the underlying color structure. Two examples are discussed: the production of rapidity gaps in dijet events at the Tevatron and heavy Higgs production via weak boson fusion at the LHC. A minijet veto for weak boson scattering at the LHC makes use of the different angular distributions and momentum scales of gluon emission in signal and background processes. It is a promising Higgs search tool.

PACS numbers: 12.15.-y, 12.38.Bx, 13.85.-t, 13.87.-a, 14.80.Bn

1. Introduction

Ever since the early 80's hadron colliders have been the accelerators with the largest available center of mass energy and hence have been of prime interest as discovery machines. New physics needs to be searched for in hard scattering events, which can be described to a large extent by the momentum distributions of jets and hard leptons or photons. The properties of the hard partons give a host of useful information on the origin of the scattering event. One recent example has been the search, and the discovery, of the top quark in $W+ \geq 3$ jet events at the Tevatron [1]. A kinematic fit to the multi-jet and jet-lepton invariant masses has allowed for the direct measurement of the top quark mass.

In this talk I want to discuss several examples where additional information can be obtained from the pattern of relatively soft partons, beyond what

* Presented at the XIX International Conference on Theoretical Physics "Particle Physics and Astrophysics in the Standard Model and Beyond", Bystra, Poland, September 19–26, 1995.

is contained in the hard jet and lepton distributions. An important case is weak boson scattering at the LHC, *i.e.* the electroweak process $qq \to qqVV$. In a weak boson scattering event no color is exchanged between the initial state quarks. Color coherence between initial and final state gluon bremsstrahlung then leads to a suppression of hadron production in the central region, between the two tagging jet candidates of the signal [2–4]. Typical backgrounds, like $t\bar{t}$ production or $q\bar{q} \to VV$ weak boson pair production, involve color exchange between the incident partons and, as a result, gluon radiation into the central region dominates. Provided these different patterns of soft gluon radiation can be distinguished, be it via soft hadronic activity or via soft jets, these different color structures can be used to separate weak boson scattering from its backgrounds.

Similar phenomena are already studied now, in dijet events at the Tevatron which are mediated by the exchange of color singlet objects in the t-channel. As a preparation for the study of gluon radiation patterns in weak boson scattering I start out, in Section 2, with a discussion of gluon radiation in quark-quark scattering. Two classes of processes need to be compared. Exchange of a single gluon, *i.e.* t-channel color octet exchange, is the prototype of a background process. On the other hand, the exchange of a color singlet object in the t-channel, be it a photon or two gluons in a color singlet state, is expected to lead to a qualitatively different gluon radiation pattern. The latter is the Low-Nussinov model for the pomeron [5] and exchange of a "hard pomeron" is used to explain the recently observed rapidity gap events at the Tevatron [6–8].

In Section 3, a more involved case will then be addressed, namely weak boson scattering at the LHC [9]. The production and subsequent decay $H \to W^+W^-$ of a heavy Higgs boson will be used as an example to discuss some of the techniques, like forward jet-tagging [10–13] or central jet vetoing [12, 13], which have been developed to distinguish weak boson scattering signals from QCD background processes. This general discussion of the hard scattering events will be followed by a look at the consequences of the different color structures of signal and background processes. In the signal, gluons are emitted at rather low transverse momenta and mainly in the forward and backward directions, leaving a central region with little hadronic activity apart from the Higgs decay products. Typical background processes emit gluons at considerably higher transverse momenta and preferentially in the central region. These differences suggest techniques like a minijet veto [14] or rapidity gaps [4] to enhance the signal versus the backgrounds. Some final conclusions will be drawn in Section 4.

2. Manifestations of color: rapidity gaps at the Tevatron

One important aspect distinguishing signal and background processes is the color flow in the contributing Feynman graphs. Many signal processes involve electroweak interactions and are thus due to the exchange of color singlet quanta while the QCD backgrounds are mediated by color octet gluon exchange. The question arises whether this different color flow has observable consequences which can then be used for background reduction. Let us start here with the simplest example possible, namely dijet production at the Tevatron, which has emerged as an unexpectedly rich QCD laboratory in recent years. The discussion will closely follow Ref. [15].

2.1. Quark-quark scattering at the tree level

A number of $2 \to 2$ subprocesses contribute to dijet production: gluon-gluon scattering, quark-gluon scattering, $q\bar{q}$ annihilation and pair production, and quark-quark or quark-antiquark elastic scattering. For simplicity let us concentrate on the Rutherford scattering process

$$q_1(p_1, i_1) Q_3(p_3, i_3) \to q_2(p_2, i_2) Q_4(p_4, i_4)\,, \tag{1}$$

where the i_n and p_n denote the colors and momenta of the quarks. The two types of SM contributions, namely color singlet γ/Z exchange and color octet gluon exchange in the t-channel are depicted in Fig. 1. Neglecting the Z contribution in the following, the matrix elements for the two cases can be written as

$$\mathcal{M}_\gamma = \delta_{i_2 i_1}\delta_{i_4 i_3}\, e_q e_Q\, A = \delta_{i_2 i_1}\delta_{i_4 i_3}\, e_q e_Q\, \frac{\overline{u}(p_2)\gamma^\mu u(p_1)\,\overline{u}(p_4)\gamma_\mu u(p_3)}{(p_1 - p_2)^2}\,, \tag{2}$$

$$\mathcal{M}_g = T^a_{i_2 i_1} T^a_{i_4 i_3}\, g^2\, A = \left(\frac{1}{2}\delta_{i_2 i_3}\delta_{i_4 i_1} - \frac{1}{2N}\delta_{i_2 i_1}\delta_{i_4 i_3}\right) g^2\, A\,. \tag{3}$$

The Kronecker deltas in $\mathcal{M}_\gamma$ describe the fact that the color of q_1 is directly transferred to q_2 while in the QCD case the exchanged gluon transmits the color of q_1 to Q_4 (to leading order in $1/N$). Does this difference in color structure lead to observable consequences?

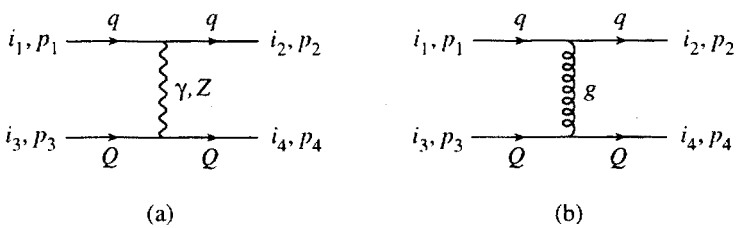

Fig. 1. Feynman graphs contributing to elastic quark-quark scattering via a) color singlet photon or Z exchange and b) color octet gluon exchange.

A qualitative understanding of these differences can be obtained by considering the acceleration of the color charges in forward scattering, at small $|t| = -(p_1 - p_2)^2 = s/2\,(1 - \cos\theta) \ll (p_1 + p_3)^2 = s$. In the case of t-channel photon exchange, quark q will be deflected by a small angle θ with respect to the original q_1 direction and so will the color charge carried by it. The acceleration of the color charge by a small angle results in gluon bremsstrahlung in the forward direction only and, similarly, the small deflection of the color charge carried by Q results in gluon radiation in the backward direction, with very little radiation between the two scattered quarks. For color octet gluon exchange, on the other hand, the color charges are exchanged between the two quarks q and Q, *i.e.* they are deflected by the large angle $\pi - \theta$, and this strong acceleration of color charges results in strong gluon bremsstrahlung at large angles, between the directions of the final state quarks.

This qualitative picture is confirmed by calculating the gluon emission corrections to qQ elastic scattering, *i.e.* by considering the process

$$q(p_1, i_1)\, Q(p_3, i_3) \longrightarrow q(p_2, i_2)\, Q(p_4, i_4)\, g(k, a)\,, \tag{4}$$

where k and a denote the gluon momentum and color. At any order of perturbation theory, the amplitude for this process can be written in terms of four orthogonal color tensors, which we denote by O_1, O_2, S_{12}, and S_{34},

$$\mathcal{M} = O_1 M_1 + O_2 M_2 + S_{12} M_{12} + S_{34} M_{34}\,. \tag{5}$$

In an $SU(N)$ gauge theory they are given explicitly by

$$S_{12} = T^a_{i_4 i_3}\, \delta_{i_2 i_1}\,, \tag{6}$$

$$S_{34} = T^a_{i_2 i_1}\, \delta_{i_4 i_3}\,, \tag{7}$$

$$O_1 = \frac{-2}{N}\,(S_{12} + S_{34}) + T^a_{i_2 i_3}\, \delta_{i_4 i_1} + T^a_{i_4 i_1}\, \delta_{i_2 i_3}\,, \tag{8}$$

$$O_2 = T^a_{i_4 i_1}\, \delta_{i_2 i_3} - T^a_{i_2 i_3}\, \delta_{i_4 i_1}\,. \tag{9}$$

S_{12} marks the process where the quark q keeps its color. Similarly, S_{34} multiplies the amplitude for t-channel color singlet exchange as viewed from quark Q. Within QCD, O_1 and O_2 correspond to t-channel color octet exchange as viewed from either of the two scattering quarks.

Let us first apply this color decomposition to the tree level QED and QCD amplitudes. The five Feynman graphs for the QCD process are shown in Fig. 2. Lumping the momentum and helicity dependence of the individual Feynman diagrams into reduced amplitudes $A^{(1)} \cdots A^{(5)}$, one obtains for the QCD amplitudes at tree level

$$M_{12}^{\mathrm{QCD}} = \frac{-g^3}{2N}\left(A^{(1)} + A^{(2)}\right) \equiv \frac{-g^3}{2N}\, A^{(12)}\,, \tag{10}$$

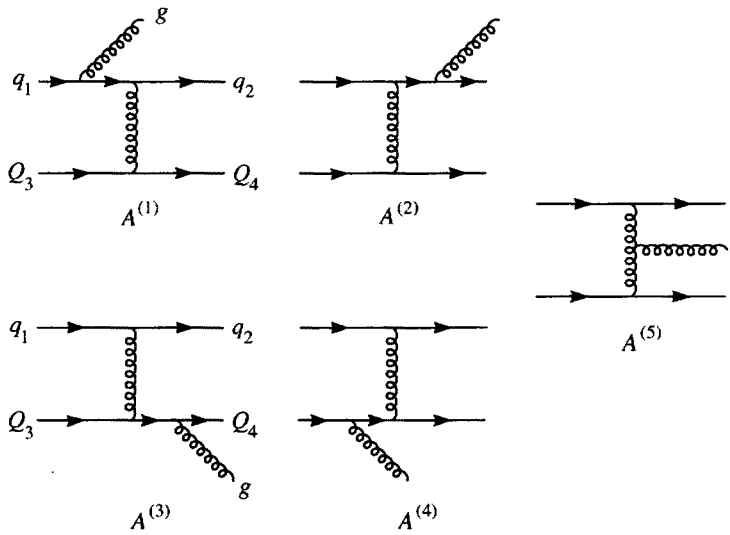

Fig. 2. Feynman graphs for the process $qQ \to qQg$ at tree level.

$$M_{34}^{\mathrm{QCD}} = \frac{-g^3}{2N}\left(A^{(3)} + A^{(4)}\right) \equiv \frac{-g^3}{2N} A^{(34)}, \tag{11}$$

$$M_1^{\mathrm{QCD}} = \frac{-g^3}{4}\left(A^{(1)} + A^{(2)} + A^{(3)} + A^{(4)}\right), \tag{12}$$

$$M_2^{\mathrm{QCD}} = \frac{-g^3}{4}\left(A^{(1)} - A^{(2)} + A^{(3)} - A^{(4)} + 2A^{(5)}\right) \equiv \frac{-g^3}{4} A^{(\mathrm{na})}. \tag{13}$$

The non-abelian three-gluon-vertex only contributes to the color octet exchange amplitude M_2. Both M_2 and M_1 vanish for t-channel photon exchange, while the color singlet exchange amplitudes are given by

$$M_{12}^{\mathrm{QED}} = -ge_q e_Q\left(A^{(3)} + A^{(4)}\right) = -ge_q e_Q A^{(34)}, \tag{14}$$

$$M_{34}^{\mathrm{QED}} = -ge_q e_Q\left(A^{(1)} + A^{(2)}\right) = -ge_q e_Q A^{(12)}, \tag{15}$$

where e_q and e_Q denote the electric charges of the two quarks.

The resulting color and polarization summed squared amplitudes,

$$\sum |\mathcal{M}|^2 = \frac{N^2-1}{2} N \times \sum_{\text{polarizations}} \left(|M_{12}|^2 + |M_{34}|^2 + 2\frac{N^2-4}{N^2}|M_1|^2 + 2|M_2|^2\right), \tag{16}$$

are shown in Fig. 3(a) for both the QCD and the QED case. Shown is the dependence of $\sum |\mathcal{M}^2|/s$ on the rapidity of the emitted gluon when all

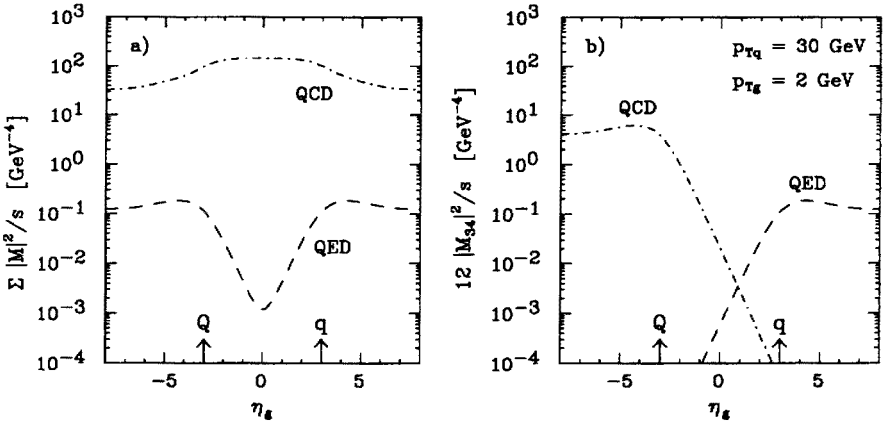

Fig. 3. Rapidity distribution of emitted gluons in $qQ \to qQg$ scattering for fixed final state parton transverse momenta of $p_{Tq} = 30$ GeV and $p_{Tg} = 2$ GeV. The quark rapidities are fixed at $\eta_q = \pm 3$ (indicated by the arrows). In part a) results are shown for the sum over all color structures for single gluon and for t-channel photon exchange. The M_{34} terms alone, in part b), demonstrate the difference between the QED and the QCD color singlet exchange terms. Quark charges are taken as $e_q = e_Q = +2/3e$.

other phase space parameters are kept fixed, namely the two quarks are held at $p_T = 30$ GeV and pseudorapidities $\eta_q = 3$ and $\eta_Q = -3$ and the gluon transverse momentum is chosen to be $p_{Tg} = 2$ GeV. The details of this choice are irrelevant: forward scattering of the two quarks is a sufficient condition to obtain the qualitative radiation pattern of Fig. 3. In the QCD case the color octet contributions, via the non-abelian amplitude $A^{(na)}$, lead to enhanced gluon emission in the angular region between the two jets. For t-channel photon exchange this region is essentially free of gluons due to color coherence between initial and final state gluon radiation [16, 17]: gluon emission into the central region is exponentially suppressed as the rapidity distance from the quarks increases.

Going beyond the parton level scattering process and considering the actual $p\bar{p}$ scattering event, hadronization of the emitted gluons will result in (soft) hadrons which will trace the angular distribution of their parent partons. In t-channel color singlet exchange, gluon radiation is severely suppressed in the angular region between the quarks, and, thus, a similar pattern of soft hadrons is expected. This leaves a rapidity gap, *i.e.* a rapidity region between the two quark jets which is essentially void of produced hadrons.

2.2. Rapidity gaps at the Tevatron

Rapidity gaps in hard dijet events have indeed been observed at the Tevatron [6–8]. The D0 Collaboration, for example, has studied events with two hard, forward and backward jets with

$$E_T > 30\ \text{GeV}\,, \qquad |\eta_j| > 2\,, \qquad \eta_1 \cdot \eta_2 < 0\,, \tag{17}$$

and has then searched for signs of hadronic activity in the pseudorapidity range between the two jets. Inside the region of width $\Delta\eta_c$ between the tangents to the two jet definition cones (of radius $R = 0.7$ in the lego-plot) D0 has then studied the hadronic multiplicity in terms of the number of active towers in the electromagnetic calorimeter, above a minimum transverse energy threshold of 200 MeV. The measured multiplicity distribution is shown in Fig. 4.

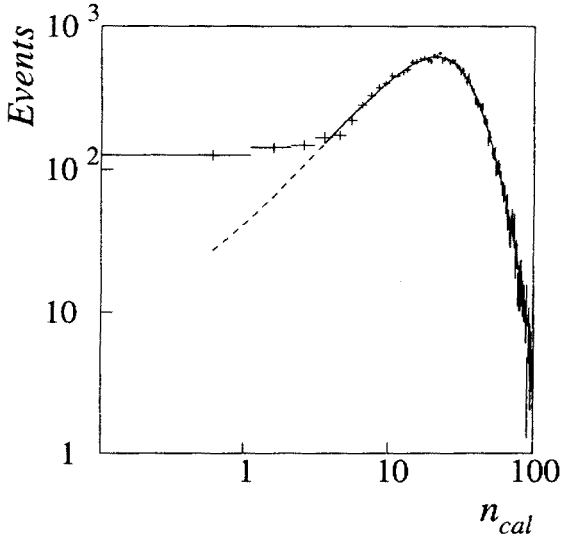

Fig. 4. Electromagnetic tower multiplicity between widely separated jets as observed by D0 [8]. Because of the logarithmic n_{cal} scale all multiplicities are shifted by +0.5 to the right. The excess of low multiplicity (rapidity gap) events above the double negative binomial fit (solid and dashed line) is due to color singlet exchange in the t-channel.

One observes a clear excess of low multiplicity events, above the expectation from extrapolating a double negative binomial distribution which fits very well the high multiplicity region. This excess corresponds to a fraction

$$f_{\mathbf{gap}} = 1.07 \pm 0.10(\text{stat})^{+0.25}_{-0.13}(\text{syst})\,\% \tag{18}$$

of rapidity gap events in dijet production. In addition, this fraction is essentially independent of $\Delta\eta_c$, for pseudorapidity separations larger than $\Delta\eta_c \approx 2$ between the jet definition cones [6]. This independence of scattering angle in the parton c.m. frame (for forward scattering) implies that the rapidity gap events follow a $1/t^2$ Rutherford scattering distribution, just like the non-gap dijet events to which they are normalized and which are dominated by single gluon exchange in the t-channel.

This angular distribution is exactly as would be expected if the gap events were produced by t-channel photon exchange. However, the observed rate is too large to be consistent with an electroweak origin. The dijet cross section from t-channel photon, Z or W exchange is between 10^{-3} and 10^{-4} of the QCD dijet cross section [18] in the phase space region considered by D0 and, hence, cannot account for the one percent fraction of dijet events which exhibit a rapidity gap.

Actually, the discrepancy is even larger because a rapidity gap, even if present at the level of a single parton collision, may be covered by double parton scattering (DPS) or, more generally, the underlying event. The hardness of the produced jets translates into an impact parameter between the scattering partons which is negligible compared to the transverse size of the incident protons. This makes it quite likely that some of the other partons in the p and the $\bar{p}$ will scatter as well, via gluon (color) exchange, and the resulting color recombination would lead to the filling of the rapidity gap. Only the fraction of dijet events without DPS or an underlying event can be expected to preserve a rapidity gap. This fraction, the survival probability P_s of rapidity gaps, has been estimated by several authors [4, 17, 19] for both the Tevatron and supercolliders and it is expected to be in the 3–30% range. For illustration I will use a value of $P_s = 10\%$ in the following. At the LHC P_s can be measured independently, by comparing the number of electroweak $qq \to qqW$ or $qq \to qqZ$ events which exhibit a rapidity gap with the SM cross sections for these processes [20].

2.3. Two gluon color singlet exchange and rapidity gaps

Given that electroweak quark scattering cannot account for the observed rate of rapidity gap events at the Tevatron, there must be a QCD source of t-channel color singlet exchange. Indeed, the exchange of two gluons in a color singlet state, as depicted in Fig. 5(b), provides a ready source and has been suggested by Low and Nussinov as the basic model for the Pomeron [5].

The rate of rapidity gap events can be understood qualitatively in terms of forward scattering by single gluon and two gluon color singlet exchange as shown in Fig. 5. The observed rate was, in fact, predicted by Bjorken [4]. For forward qq scattering the matrix elements for the dominant helicity

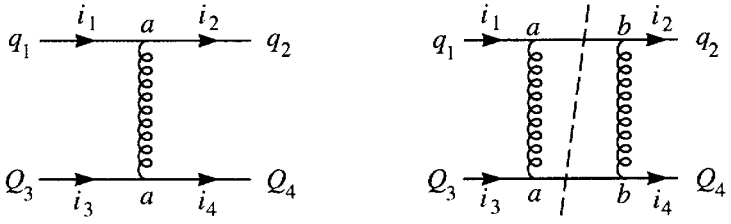

Fig. 5. Feynman graphs for quark scattering via (a) single gluon exchange and (b) exchange of two gluons in a color singlet state.

configurations are given by

$$\mathcal{M}_g \approx \frac{8\pi\alpha_s\hat{s}}{Q^2}\, T^a_{i_2 i_1}\, T^a_{i_4 i_3} \tag{19}$$

for single gluon exchange, while color singlet two gluon exchange is dominated by the imaginary part of the amplitude in the forward region,

$$\begin{aligned}\mathcal{M}_{\mathbf{singlet}} &\approx i\,\frac{8\pi\alpha_s\hat{s}}{Q^2}\,\frac{\alpha_s}{2}\log(Q^2R^2)\,\left((T^bT^a)_{i_2 i_1}\,(T^bT^a)_{i_4 i_3}\right)_{\mathbf{singlet}} \\ &= i\,\frac{8\pi\alpha_s\hat{s}}{Q^2}\,\frac{\alpha_s}{2}\log(Q^2R^2)\,\mathrm{Tr}(T^bT^a)\frac{\delta_{i_2 i_1}}{3}\,\mathrm{Tr}(T^bT^a)\frac{\delta_{i_4 i_3}}{3}\,. \end{aligned} \tag{20}$$

Here R is a cutoff parameter, of the order of the proton radius, which is needed because the intermediate phase space integral for the Feynman graph in Fig. 5(b) is infrared divergent. The fraction of two gluon color singlet exchange events is then given by

$$\begin{aligned}\frac{\hat{\sigma}_{\mathbf{singlet}}}{\hat{\sigma}_g} &= \frac{\frac{4}{9}|\mathrm{Im}\mathcal{M}_{\mathbf{singlet}}|^2}{2|\mathcal{M}_g|^2} = \frac{2}{9}\left|\frac{1}{2}\log(Q^2R^2)\,\alpha_s(Q^2)\right|^2 \\ &\approx \frac{2}{9}\left|\frac{1}{2}\log(Q^2R^2)\,\frac{12\pi}{(33-2n_f)\,\log\frac{Q^2}{\Lambda^2_{\mathrm{QCD}}}}\right|^2\,, \end{aligned} \tag{21}$$

where we have used the LO formula for the running coupling constant at the scale Q^2 which is the physical scale of the process. For sufficiently large momentum transfer $Q^2 = |\hat{t}|$ the two logs are approximately equal and one finds a constant color singlet exchange fraction,

$$\frac{\hat{\sigma}_{\mathbf{singlet}}}{\hat{\sigma}_g} \approx \frac{1}{2}\left|\frac{4\pi}{33-2n_f}\right|^2 \approx 0.15\,, \tag{22}$$

for $n_f = 5$. Thus about 15% of all quark-quark scattering events are due to color singlet two gluon exchange and may lead to a rapidity gap, provided that no underlying event is present. The probability for the latter is given by the survival probability P_s and thus the expected fraction of dijet events from quark-quark scattering with an observable rapidity gap is expected to be [4]

$$f_{qq} = \frac{d\sigma_{qq,\mathbf{gap}}/dt}{d\sigma_{qq,\mathbf{dijet}}/dt} \approx 0.15\, P_s \approx 0.015\,, \tag{23}$$

which agrees well with the D0 value of 0.0107. This agreement, however, is at least partially by accident. In the forward scattering region, the imaginary parts of the color singlet exchange amplitudes in quark-gluon and gluon-gluon scattering are the same as the quark-quark scattering amplitude, except for a color factor [4],

$$\mathrm{Im}\,\mathcal{M}_{gg,\mathbf{singlet}} = \frac{9}{4}\,\mathrm{Im}\,\mathcal{M}_{qg,\mathbf{singlet}} = \left(\frac{9}{4}\right)^2 \mathrm{Im}\,\mathcal{M}_{qq,\mathbf{singlet}}\,, \tag{24}$$

and, at small t, the same proportionality is found for the single gluon exchange cross sections,

$$\frac{d\sigma_{gg}}{dt} = \frac{9}{4}\,\frac{d\sigma_{qg}}{dt} = \left(\frac{9}{4}\right)^2 \frac{d\sigma_{qq}}{dt}\,. \tag{25}$$

Since the singlet exchange cross section is proportional to $(\mathrm{Im}\,\mathcal{M}_{singlet})^2$, the gap fractions for the three channels are related by

$$f_{gg} \approx \frac{9}{4} f_{qg} \approx \left(\frac{9}{4}\right)^2 f_{qq}\,, \tag{26}$$

and, thus, the fraction of color singlet exchange events is substantially larger than the 15% expected for quark-quark scattering alone. Using the measured rapidity gap fraction of $\approx 1\%$ this in turn indicates a survival probability well below 10% for the Tevatron.

The rate estimates above assume that two gluon color singlet exchange, *i.e.*the exchange of a Low-Nussinov pomeron, does indeed lead to the same kind of gluon radiation pattern as t-channel photon exchange and, thus, can produce a rapidity gap after hadronization. However, the intermediate phase space integral for the Feynman graph of Fig. 5(b) is dominated by the phase space region where one of the exchanged gluons is very soft. Thus the color of the other, hard gluon is screened at large distances, *i.e.* the Low-Nussinov pomeron is an extended object with colored constituents. As a result, analogy to single photon exchange may be misleading: gluon

radiation may resolve the internal color structure of the pomeron. In order to answer this question we need to find out whether real gluon emission in Low-Nussinov pomeron exchange follows the pattern typical for t-channel gluon exchange or photon exchange [15]. Only in the second case can we expect Low-Nussinov pomeron exchange to lead to rapidity gaps.

We already have studied the general color structure of the process $q_{i_1}Q_{i_3} \to q_{i_2}Q_{i_4}g^a$. The amplitude contains two color octet pieces M_1 and M_2 and the color singlet exchange amplitudes M_{12} and M_{34}. Let us concentrate on the last one, which describes color singlet exchange as seen by quark Q. Even for t-channel gluon exchange does this color singlet amplitude exist. However, the rapidity distribution of the emitted gluon is markedly different from photon exchange.

In the QED case the M_{34} amplitude corresponds to emission of the final state gluon off the quark q ($A^{(1)}$ and $A^{(2)}$ in Fig. 2). In forward scattering ($\eta_q = +3$ in Fig. 3(b)) the gluon is radiated between the initial and final state q directions, *i.e.* at $\eta_g \gtrsim \eta_q$. The color i_1 of the initial quark q is thus transferred to a low mass color triplet object which emerges close to the beam direction. At lowest order this is the final state q, at $\mathcal{O}(\alpha_s)$ it is the qg system. The situation is thus stable against gluon emission at even higher order for the QED case and gluon radiation is suppressed in the rapidity range between the two final state quarks.

In the QCD case M_{34} corresponds to emission of the gluon from the quark Q. The gluon is preferentially emitted between the initial and the final Q directions, at $\eta_g \lesssim \eta_Q$ (dash-dotted line in Fig. 3(b)). Thus the color triplet qg system, into which the initial quark q evolves, consists of a widely separated quark and gluon. Higher order corrections will lead to strong gluon radiation into the angular region between the two and thus also into the rapidity range between the two final state quarks.

These typical patterns found for t-channel color singlet and color octet exchange can now be used as a gauge for the radiation pattern produced in $qQ \to qQg$ scattering via the exchange of two gluons in a color singlet state. In the lowest order process, $qQ \to qQ$, the color singlet exchange amplitude is dominated by its imaginary part [21]. Hence, we may estimate the radiation pattern by calculating the imaginary part of the gluon emission amplitude M_{34} only. Typical Feynman graphs are shown in Fig. 6. Details of the calculation are given in Ref. [15].

For massless internal gluon propagators the phase space integrals over the qQ, qg, and gQ intermediate states are divergent. They can be regularized by replacing the massless gluon propagator by a version which avoids unphysical gluon propagation over long distances [22]. QCD Pomeron models of this kind have been found to give a good description of available data [23]. These refinements are approximated by using an effective gluon

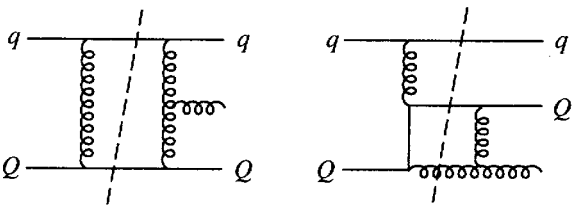

Fig. 6. Two of the 31 Feynman graphs contributing to the imaginary part of the color singlet exchange amplitude M_{34}.

mass of $m_r = 300$ MeV in the calculation.

A second problem arises because some of the contributions to $\mathrm{Im}M_{34}$ correspond to $q \to g$ splitting and subsequent $gQ \to gQ$ scattering via pomeron exchange. These contributions cannot be expected to be suppressed when the gluon is emitted between the q and the Q directions and thus would mask the radiation off pomeron exchange in qQ scattering. These splitting contributions have been subtracted in Ref. [15] to yield the square of the pomeron exchange radiation pattern, $|\mathrm{Im}M_{34}^{\mathrm{pom}}|^2$, which is shown in Fig. 7.

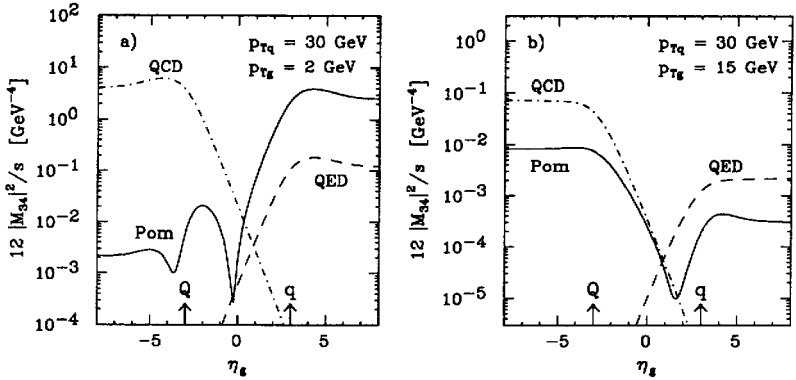

Fig. 7. Rapidity distribution of emitted gluons in $uc \to ucg$ scattering via two gluon color singlet exchange as seen by the charm quark. The phase space parameters for the quarks are the same as in Fig. 3 and results are shown for a) the case of a soft gluon ($p_{Tg} = 2$ GeV) and b) a hard gluon ($p_{Tg} = 15$ GeV). For comparison tree level results are shown for gluon (dash-dotted lines) and photon exchange (dashed lines).

For high transverse momentum of the emitted gluon (of order of the quark momenta, see Fig. 7(b)) the radiation pattern is quite similar to the one obtained for single gluon exchange. Hard emitted gluons have too short a wavelength to see the screening of the color charge of the harder

exchanged gluon by the second, typically very soft, exchanged gluon. The Low-Nussinov pomeron thus reveals itself as an extended object. Hard gluon emission is able to resolve the internal color structure of the pomeron. As the transverse momentum of the emitted gluon is decreased, a qualitative transition occurs, as is apparent by comparing the $p_{\mathrm{T}g} = 2$ GeV and 15 GeV cases in Fig. 7. The gluon radiation has too long a wavelength to resolve the internal color structure and hence the pomeron appears as a color singlet object.

In dijet production at the Tevatron, in the kinematic range studied by D0, gluon radiation will be dominated by the soft region, with transverse gluon momenta in the few GeV range or below, as shown in Fig. 7(a). The emission of these soft gluons follows a pattern very similar to the one observed for t-channel photon exchange, which leads to the formation of rapidity gaps. One concludes that two gluon color singlet exchange in dijet events does indeed lead to the formation of rapidity gap events as observed at the Tevatron.

3. Weak boson scattering

One of the major reasons for building a hadron supercollider is the study of weak boson interactions in the TeV range. Within the forseeable future this task will have to be performed in pp collisions at 14 TeV at the Large Hadron Collider (LHC) at CERN. Because of its limited energy the study of weak boson scattering will be a very demanding task at the LHC, requiring a full arsenal of tools to isolate $qq \to qqVV$ weak boson scattering events from the backgrounds. For example, jets will have to be used as a tagging device (as in the top quark search at the Tevatron) and rapidity gap techniques, *i.e.* the exploitation of the t-channel color singlet exchange in the signal, should prove useful as well. Before considering the benefits of these techniques in weak boson scattering and the search for a heavy Higgs at the LHC, let us start with a brief note on the physics of a strongly interacting Higgs sector.

3.1. Higgs production and longitudinal weak boson scattering [24]

In a more general context, the search for the Higgs boson is part of the quest for the basic interactions which are responsible for the spontaneous breaking of the SU(2)×U(1) gauge symmetry. The existence of this local symmetry is evidenced by the observation of W and Z bosons and the fact that their experimentally determined couplings to quarks and leptons agree with the gauge theory predictions. The appearance of gauge boson masses then requires the gauge symmetry to be broken spontaneously, with some

order parameter Φ acquiring a vacuum expectation value (v.e.v.). The fact that the W to Z mass ratio leads to a ρ-parameter very close to unity finally tells us that this order parameter must transform essentially as an SU(2)-doublet.

Beyond these basic facts the precise nature of the order parameter and of the interactions which drive its v.e.v. must be determined experimentally. Within the SM the order parameter is simply the scalar Higgs doublet field,

$$\Phi = \begin{pmatrix} \frac{1}{\sqrt{2}}\left(v + H + i\chi^3\right) \\ i\chi^- \end{pmatrix}, \tag{27}$$

where v is the Higgs v.e.v., $\chi^{\pm}$ and χ^0 are the Goldstone bosons which are closely related to the longitudinal degrees of freedom of the $W^{\pm}$ and the Z, and H is the field describing the physical Higgs boson which we would like to detect experimentally.

Without spontaneous breakdown of the symmetry, SU(2)×U(1) gauge invariance forbids any mass terms for the known quarks and leptons as well as for the gauge bosons. Thus these masses must be proportional to the v.e.v. Since v appears only in the combination $v + H$ in the SM (see Eq. (27)), this implies couplings of the fermions and gauge bosons to the Higgs which are proportional to the masses of the former. Let us consider the most important of these, the couplings of the Higgs to the gauge bosons and to the top quark. They are derived from the kinetic energy term for the Higgs doublet field and from the Yukawa coupling of the Higgs field to the top-bottom doublet, $T = (t_{\mathrm{L}}, b_{\mathrm{L}})^T$, and the right handed top quark field, t_{R},

$$\begin{aligned}
\mathcal{L} &= (D_\mu \Phi)^\dagger (D^\mu \Phi) - (\lambda_t \overline{T} \Phi t_{\mathrm{R}} + \mathrm{h.c.}) \\
&= \left(1 + \frac{H}{v}\right)^2 \left| \frac{i}{2} \begin{pmatrix} g W_\mu^3 - g' B_\mu & \dots \\ g\sqrt{2} W_\mu^- & \dots \end{pmatrix} \begin{pmatrix} \frac{v}{\sqrt{2}} \\ 0 \end{pmatrix} \right|^2 \\
&\quad - \left(1 + \frac{H}{v}\right) \lambda_t \bar{t}_{\mathrm{L}} \frac{v}{\sqrt{2}} t_{\mathrm{R}} + \dots \\
&= \left(1 + \frac{H}{v}\right)^2 \left(m_W^2 W_\mu^\dagger W^\mu + \frac{m_Z^2}{2} Z_\mu Z^\mu \right) \\
&\quad - m_t \bar{t}_{\mathrm{L}} t_{\mathrm{R}} \left(1 + \frac{H}{v}\right) + \dots ,
\end{aligned} \tag{28}$$

which gives relations between the masses and coupling constants,

$$m_W = \frac{gv}{2}, \qquad m_Z = \frac{gv}{2\cos\theta_W}, \qquad m_t = \frac{\lambda_t v}{\sqrt{2}}. \tag{29}$$

The interaction terms of Eq. (28) imply that the Higgs boson decays predominantly into the heaviest particles available. For the heavy Higgs scenario, which is considered in the following, these are the decay modes $H \to W^+W^-$, $H \to ZZ$, and $H \to \bar{t}t$. For a Higgs mass of 800 GeV, for example, the corresponding branching ratios are

$$B(H \to W^+W^-) \approx 0.59\,, \quad B(H \to ZZ) \approx 0.29\,, \quad B(H \to \bar{t}t) \approx 0.12\,, \tag{30}$$

and the total Higgs decay width is expected to be about 290 GeV. In order to exploit the dominant decay modes, one needs to search for the Higgs signal in W^+W^- and ZZ production events at the LHC, with subsequent leptonic decays of at least one of the weak bosons.

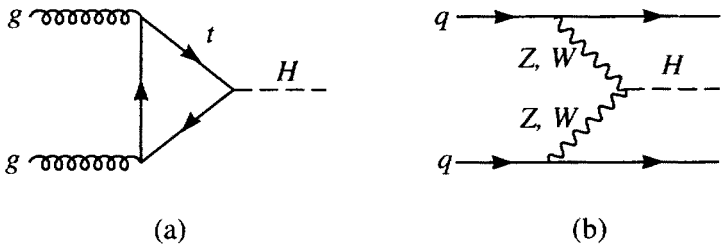

Fig. 8. Feynman graphs for the two dominant Higgs production processes at the LHC, (a) gluon-gluon fusion via a top-quark loop and (b) weak boson fusion.

Similar to the Higgs decay modes, the dominant production processes involve heavy particles. At LHC energy, the Higgs boson is mainly produced via gluon fusion, $gg \to H$, which proceeds via a top quark loop and is depicted in Fig. 8(a), and via weak boson fusion, $WW,\ ZZ \to H$, which, more precisely, is the electroweak process $qq \to qqH$ (see Fig. 8(b)). The corresponding production cross sections are shown in Fig. 9.

While the gluon fusion cross section ranges from 30 to 0.5 pb for 100 GeV $< m_H <$ 800 GeV, weak boson fusion rates are typically smaller by a factor 2.5 to 10, the difference becoming smallest at large Higgs boson masses. This somewhat smaller cross section, however, is compensated by a number of features which are special to the weak boson scattering process. First of all the additional two final state quarks will frequently manifest themselves as hadronic jets which allows to suppress backgrounds by jet-tagging. Second the two production processes probe different interactions of the Higgs boson. The gluon fusion cross section is proportional to λ_t^2, *i.e.* it measures the Yukawa coupling of the produced scalar to the top quark. This Yukawa coupling, however, does not identify the produced particle as being connected to the symmetry breaking mechanism, it is possible for a generic scalar particle. The HVV coupling, on the other hand, at tree level,

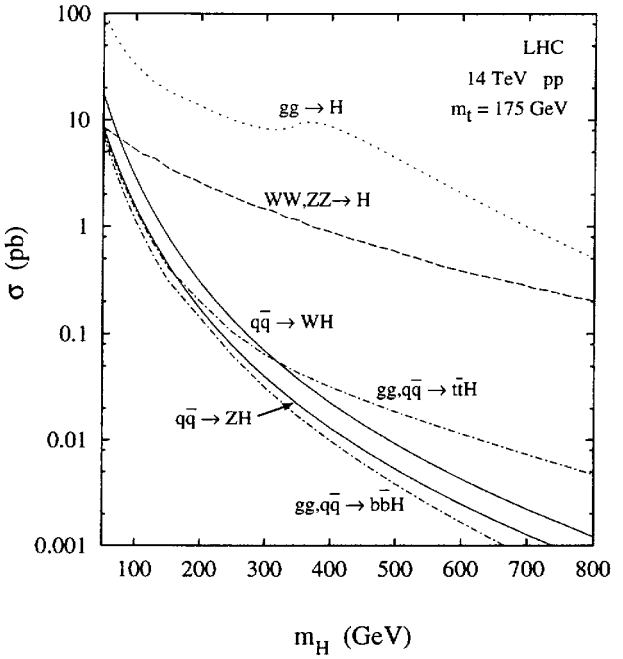

Fig. 9. Production cross sections for the SM Higgs boson at the LHC. From Ref. [25].

is only possible if H is indeed the Higgs boson. The weak boson fusion rate directly measures the HVV coupling (as does the $H \to VV$ decay width) and thus one would like to measure both gluon and weak boson fusion cross sections in order to disentangle the various couplings of H in Eq. (28).

When considering the full processes $qq \to qqWW$ or $qq \to qqZZ$, the resonance approximation, *i.e.* considering graph (b) in Fig. 8 only, is only valid for a Higgs width $\Gamma_H << m_H$. For a heavy (and wide) Higgs resonance the $VV \to H(\to VV)$ subprocess in Fig. 8(b) must be replaced by the full weak boson scattering amplitude, as depicted in Fig. 10 for the process $ZZ \to WW$. In addition, weak boson bremsstrahlung off the quark lines must be considered [26, 13].

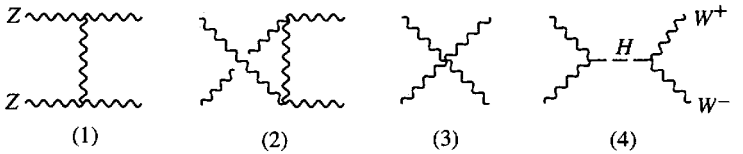

Fig. 10. Feynman graphs for the weak boson scattering process $ZZ \to W^+W^-$.

Very strong cancellations between the various Feynman graphs of Fig. 10 appear when all the external vector bosons are longitudinally polarized [27]. The isospin and angular momentum zero contributions from the first two graphs and from the third graph individually grow as $\hat{s}^2/m_W^4$. However, the leading terms cancel when the sum of the three graphs is considered. Even the $\hat{s}/m_W^2$ growth of their sum, however, would lead to a violation of partial wave unitarity at a $\sqrt{\hat{s}}$ of about 1 TeV. At high energies, above $\hat{s} = m_H^2$, it is the destructive interference with the fourth graph, s-channel Higgs exchange, which leads to an acceptable $J = I = 0$ partial wave amplitude. Thus the existence of the Higgs boson, or some other, additional contribution to the weak boson scattering amplitude, beyond the vector boson self-coupling graphs (1)–(3) in Fig. 10, is required by unitarity of the S-matrix [27]. This additional contribution does not have to be the s-channel exchange of a scalar object. It might be the t- or u-channel exchange of a vector particle which resides in a weak isospin triplet, like in technicolor models. Or nature may have realized the unitarization of the weak boson scattering amplitudes in yet another manner [9].

Depending on which path is realized in nature, the various weak boson scattering processes like $W^+W^- \to W^+W^-$, $WZ \to WZ$, $W^+W^+ \to W^+W^+$, *etc.* will exhibit markedly different magnitude and shape (energy dependence) of the cross sections. If a technirho existed, the WZ channel, for example, would exhibit a resonance at the technirho mass, while this channel has a small cross section if a $J = I = 0$ scalar is responsible for the unitarization of the S-matrix (as in the SM). Thus the study of all weak boson scattering channels is important in order to fully probe the symmetry breaking sector. In the following I will use the search for a SM heavy Higgs to discuss techniques of background suppression. One should keep in mind, however, that these methods are more general and can be applied to study any of the weak boson scattering processes.

3.2. Forward jet-tagging

A characteristic feature of weak boson scattering events are the two accompanying quarks (or antiquarks) from which the "incoming" Ws or Zs have been radiated (see Fig. 8(b)). In general these scattered quarks will give rise to hadronic jets. By tagging them, *i.e.* by requiring that they are observed in the detector, one hopes to obtain a powerful background rejection tool [10, 11]. Whether such an approach can be successful depends on the properties of the tagging jets: their typical transverse momenta, their energies, and their angular distributions.

Similar to the emission of virtual photons from a high energy electron beam, the incoming weak bosons tend to carry a small fraction of the incoming parton energy [28]. At the same time the incoming weak bosons

must carry substantial energy, of order $m_H/2 = m_{VV}/2$, in order to produce a weak boson pair of large invariant mass. Thus the final state quarks in $qq \to qqVV$ events will carry very high energies, of order 1 TeV or even higher. This is to be contrasted with their transverse momenta, which are of order $p_T \approx m_W$. This low scale arises because the weak boson propagators in Fig. 8(b) introduce a factor

$$D_V(q^2) = \frac{-1}{q^2 - m_V^2} \approx \frac{1}{p_T^2 + m_V^2} \tag{31}$$

into the production amplitudes and suppress the $qq \to qqH$ cross section for quark transverse momenta above m_V. The modest transverse momentum and high energy of the scattered quark corresponds to a small scattering angle, typically in the $1.5 < \eta < 4.5$ pseudorapidity region.

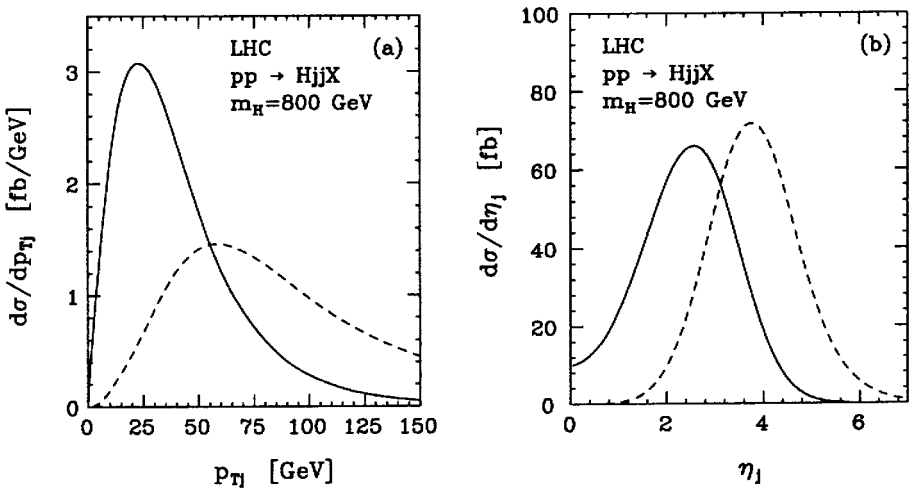

Fig. 11. Transverse momentum and pseudorapidity distributions of the two (anti)quark jets in $qq \to qqH$ events at LHC energy. Shown are (a) $d\sigma/dp_{Tj}$ for the highest (dashed curve) and lowest p_T jet (solid curve) and (b) $d\sigma/d|\eta_j|$ for the most forward (dashed curve) and the most central jet (solid curve).

These general arguments are confirmed by Fig. 11, where the transverse momentum and pseudorapidity distributions of the two potential tagging jets are shown for the production of a $m_H = 800$ GeV Higgs boson at the LHC. One finds that one of the two quark jets has substantially lower median p_T (≈ 30 GeV) than the other (≈ 80 GeV). As a result, double jet-tagging, *i.e.* the requirement that both scattered quarks are visible as jets, proves quite costly [11–13] unless jets with transverse momenta around 30 GeV can be identified in the forward region. A different approach is

single forward jet-tagging which relies only on the higher p_T tagging-jet and thus proves more effective for higher transverse momentum thresholds [12, 13, 29, 30].

This transverse momentum threshold needs to be set such that the probability for seeing a fake tagging-jet becomes small. At full LHC luminosity of $\mathcal{L} = 10^{34}\text{cm}^{-2}\text{sec}^{-1}$ one of the most important sources of such background jets are additional $pp \to jjX$ events in the same bunch crossing as the $pp \to VVX$ signal event. With a bunch crossing happening every 25 nsec, a process with a cross section of $\sigma_{\text{eff}} = [\mathcal{L}\ 25\text{nsec}]^{-1} = 4$ mb will, on average, happen during each bunch crossing. Using Poisson statistics, the probability to get a random jet of transverse momentum $p_{Tj} > p_{T,\text{cut}}$ in any event previously selected is then given by

$$P_j(p_{T,\text{cut}}) = 1 - \exp\left(-\frac{\sigma_{jj}(p_{Tj} > p_{T,\text{cut}})}{\sigma_{\text{eff}}}\right) \approx \frac{\sigma_{jj}(p_{Tj} > p_{T,\text{cut}})}{\sigma_{\text{eff}}}\,. \quad (32)$$

With single-jet cross sections of about 0.5–1 mb above $p_{Tj} = 20$ GeV in the relevant rapidity range, overlapping events in a single bunch crossing may produce fake tagging jets above 20 GeV p_T with about 15–25% probability. This estimate agrees with the results of a more detailed analysis of overlapping events at the LHC [31].

In the following let us sidestep this question of how low a transverse momentum threshold can be achieved in forward jet-tagging. By restricting ourselves to single forward jet-tagging the jet p_T threshold can be set high enough to avoid the fake jet problem from overlapping events. As an example we will consider the search for $H \to W^+W^- \to \ell^+\nu\ell^-\bar{\nu}$ decays as discussed in Ref. [14]. This particular decay mode suffers from severe backgrounds due to $t\bar{t} \to W^+W^-b\bar{b}$ decays as well as $q\bar{q} \to W^+W^-$ events (referred to as WW QCD background in the following) and thus is well suited to assess the power of jet-tagging and minijet veto techniques.

Since we are interested in the decay of a very heavy Higgs boson, the two charged W decay leptons will emerge with high transverse momentum, in the central region of the detector, and they will be well isolated from additional jets. Thus we require the presence of two charged leptons ($\ell = e, \mu$) with

$$p_{T\ell} > 50\ \text{GeV}\,, \quad |\eta_\ell| < 2\,, \quad R_{\ell j} = \sqrt{(\eta_\ell - \eta_j)^2 + (\Phi_\ell - \Phi_j)^2} > 0.7\,. \quad (33)$$

Here $p_{T\ell}$ denotes the lepton transverse momentum and η_ℓ is its pseudorapidity. The $R_{\ell j} > 0.7$ separation cut forbids a parton (jet) of $p_T > 20$ GeV in a cone of radius 0.7 around the lepton direction.

The lepton p_T cut in Eq. (33) is not in itself sufficient to focus on the production of two W's of large transverse momenta and large W-pair invariant

mass. A variable which helps to substantially suppress W bremsstrahlung backgrounds is $\Delta p_{T\ell\ell}$, the difference of the charged lepton transverse momentum vectors [30]. We thus require

$$\Delta p_{T\ell\ell} = |\mathbf{p}_{T\ell_1} - \mathbf{p}_{T\ell_2}| > 300\,\text{GeV}\,, \qquad m_{\ell\ell} > 200\,\text{GeV}\,. \tag{34}$$

The additional cut on the dilepton invariant mass removes possible backgrounds from Z leptonic decays. It is largely superceded by the the $\Delta p_{T\ell\ell}$ cut, however.

Cross sections for events satisfying the lepton acceptance criteria of Eqs. (33), (34) are listed in the first column of Table I for the case of a $m_H = 800$ GeV Higgs boson and the $q\bar{q} \to W^+W^-$ and $t\bar{t}$ production backgrounds. In the calculation of the $qq \to qqWW$ signal all W bremsstrahlung graphs have been included [26, 13] since the narrow Higgs width approximation is not appropriate any more for the large masses considered here. These additional graphs introduce an "electroweak background" which is the same as in the case of a light Higgs boson. Since a light Higgs cannot decay via $H \to WW$, we can use the SM $qq \to qqWW$ cross section for, say, $m_H = 100$ GeV as an estimate of this electroweak background. The heavy Higgs signal is then defined as $B\sigma_{SIG} = B\sigma(m_H) - B\sigma(m_H = 100\,\text{GeV})$.

TABLE I

Signal and background cross sections $B\sigma$ (in fb) for the Higgs search in $qq \to qqWW$, $WW \to \ell\nu\ell\nu$ events. Results are shown for increasingly stringent cuts. From Ref. [14].

	lepton cuts only [Eq. (33)–(34)]	+ tagging jet [Eq. (35)]	+ lepton-tagging jet separation [Eq. (36)]	+ minijet veto ($p_{T,\text{veto}} =$ 20 GeV) [Eq. (38)]
$WW(jj)$	27.4	1.73	0.57	0.13
$t\bar{t}(jj)$	640	57	25	0.47
$m_H = 100$ GeV	1.18	0.56	0.29	0.18
$m_H = 800$ GeV	3.4	1.79	1.31	0.97
signal:				
$m_H = 600$ GeV				0.78
$m_H = 800$ GeV	2.2	1.23	1.02	0.79
$m_H = 1$ TeV				0.62

Without any jet tagging the backgrounds are overwhelming: the top quark background alone exceeds the signal by a factor of 300. How much does this situation improve by forward jet-tagging? A large fraction of

the signal (55%) is retained by requiring the existence of a very energetic, forward jet of moderate p_T, in the phase space region

$$E_j^{\mathbf{tag}} > 500\,\mathrm{GeV}\,, \quad 1.5 < |\eta_j^{\mathbf{tag}}| < 4.5\,, \quad p_{Tj}^{\mathbf{tag}} > 50\,\mathrm{GeV}\,. \tag{35}$$

In addition the tagging-jet should be well separated from the W decay leptons,

$$\min |\eta_j^{\mathbf{tag}} - \eta_\ell| > 1.7\,, \tag{36}$$

Since we are now requiring additional jet activity, the previous background calculations are not sufficient any more. Rather $\mathcal{O}(\alpha_s)$ real emission corrections must be considered, *i.e.* $t\bar{t}j$ production and processes like $q\bar{q} \to W^+W^-g$ and $qg \to W^+W^-q$ need to be considered at this level. The signal and background cross sections after the cuts of Eqs (35) and (36) are listed in the second and third columns of Table I, respectively. Single forward jet-tagging has reduced the backgrounds by a factor 25–50, while keeping 45% of the signal. This reduction factor is almost sufficient for the WW QCD background, but an additional large suppression factor is needed for the top quark decays. Fortunately, the b-quarks in $t \to bW$ decay frequently give rise to additional jets and a veto on them [12], above $p_{Tb} = 25$ GeV, will substantially reduce this background [13]. One needs to be careful, however, since at such low transverse momenta the production of minijets via the emission of additional gluons cannot be neglected at the LHC.

3.3. Rapidity gaps and minijet veto

The most rigorous veto on b-quarks from top decays would be a rapidity gap requirement [2, 4] as discussed for dijet events at the Tevatron in Section 2.2. A rapidity gap trigger, *i.e.* the selection of events without any hadronic activity in some rapidity range around the two charged leptons which arise from the two Ws, would make maximal use of the different color structure of signal and background processes. In a weak boson scattering event no color is exchanged between the initial state quarks. Color coherence between initial and final state gluon bremsstrahlung then leads to a suppression of hadron production in the central region, between the two scattered quarks [2–4]. The $t\bar{t}$ production and WW QCD backgrounds, on the other hand, involve color exchange between the incident partons and, as a result, gluon radiation into the central region dominates. This gluon radiation then results in substantial hadronic activity in the vicinity of the W decay leptons.

While a rapidity gap trigger should suppress the backgrounds well below the signal level, it is not practical at the LHC, due to the small signal rate

and small survival probability of the signal. In order for a rapidity gap to be visible no additional scattering process may occur in the detector at the same time, neither in the same pp collision which produces the Higgs boson, nor by other proton pairs which collide in the same bunch crossing. The first condition is parametrized by the survival probability, P_s, which was discussed in Section 2.2, and which we expect to be below 10% at the LHC [4, 17, 19]. The second condition implies that one must run the LHC well below design luminosity, at an average of one pp scattering event per bunch crossing, or about $\mathcal{L} = 5 \cdot 10^{32}\text{cm}^{-2}\text{sec}^{-1}$. Even at this low luminosity only $P_1 = e^{-1} = 37\%$ of all bunch crossings have exactly one pp scattering event, leading to an effective yearly integrated luminosity of about 2 fb^{-1}. Given the signal cross section of 1.02 fb in the third column of Table I and an (optimistic) survival probability of $P_s = 10\%$, one would register only one Higgs signal event every five years! Note that the cuts imposed on the leptons and tagging jet are not responsible for this negative result: 22% of all signal events are accepted by them [14]. It is the combination of small survival probability and additional effective luminosity reduction by a factor 50 which kills the signal. Given the small weak boson scattering cross section, any rapidity gap strategy at the LHC must raise this effective survival probability from 1/500 to something of order unity, *i.e.* it must work at full design luminosity and must tolerate the presence of an underlying event.

The way out may be to use minijets rather than soft hadrons to define the rapidity gap. Beyond the different angular distributions of gluons in signal and background events, a second distinction is the momentum scale Q of the hard process which governs the radiation. In longitudinal weak boson scattering the color charges, carried by the incident quarks, receive momentum transfers given by the transverse momenta of the final state quarks, which typically are in the $Q = 30$ to 80 GeV range. For the background processes, on the other hand, the color charges receive a much larger momentum kick, of the order of the weak boson pair mass or even the parton center of mass energy of the event, *i.e.* $Q \approx 1$ TeV. Extra parton emission is suppressed by a factor $f_s = \alpha_s \ln (Q^2/p_{\text{T,min}}^2)$, where $p_{\text{T,min}}$ is the minimal transverse momentum required for a parton to qualify as a jet. The jet transverse momentum scale below which multiple minijet emission must be expected is set by $f_s = \mathcal{O}(1)$, and this scale is in the 30–50 GeV range for the backgrounds but well below 10 GeV for the signal.

For a more precise determination of the typical minijet p_{T} scale we must carry signal and background calculations still one order (in α_s) higher, *i.e.* the emission of one additional parton must be included. Thus we are led to consider $qq \to qqWWg$ and crossing related processes [32] for the weak boson scattering signal, and for the backgrounds $t\bar{t}jj$ events [33] and $WWjj$

events [34] must be simulated. The results of these calculations confirm the qualitative arguments made above. For the hard lepton and tagging-jet cuts of Eqs. (33)–(36), the $WWjj$ cross section, for example, is equal to the lowest order WWj cross section for a minimal parton transverse momentum of 37 GeV. Thus multiple minijets in the 20–50 GeV range are expected for the WW QCD background. Similar results are found for the $t\bar{t}$ background while this "saturation scale" for the signal is well below 10 GeV.

For a quantitative estimate of the minijet emission probability, we must use the higher order programs (which include emission of soft partons) in regions of phase space where the $n+1$ jet cross section saturates the rate for the hard process with n jets. As the p_{T} of the softest jet is lowered to values where $\sigma(n+1 \text{ jet}) \simeq \sigma(n \text{ jet})$, fixed order perturbation theory breaks down and multiple soft gluon emission (with resummation of collinear singularities into quark and gluon structure functions, *etc.*) needs to be considered in a full treatment. For the complex processes considered here such calculations are not yet possible. Instead one can employ the so called "truncated shower approximation" (TSA) to normalize the higher order emission calculations [35]. The tree-level $n+1$ jet differential cross section $d\sigma(n+1\ j)_{\mathrm{TL}}$ is replaced by

$$d\sigma(n+1\ j)_{\mathrm{TSA}} = d\sigma(n+1\ j)_{\mathrm{TL}} \left(1 - \exp\left(\frac{-p_{\mathrm{T}j,\mathbf{min}}^2}{p_{\mathrm{TSA}}{}^2}\right)\right), \qquad (37)$$

with the parameter p_{TSA} properly chosen to correctly reproduce the lower order n jet cross section when integrated over a given phase space region of this hard process. Here $p_{\mathrm{T}j,\mathbf{min}}$ is the smallest transverse momentum of any of the final state massless partons. As $p_{\mathrm{T}j,\mathbf{min}} \to 0$ the final factor in Eq. (37) acts as a regulator, which allows to integrate the $n+1$ parton cross section over the full phase space region and simulate n-jet and $n+1$-jet events simultaneously.

The results of such a calculation [14] are depicted in Fig. 12. The angular distribution of the jet (parton with $p_{\mathrm{T}} > 20$ GeV) which is closest to the leptons (more precisely, closest to the average lepton rapidity $\bar{\eta} = (\eta_{\ell^+} + \eta_{\ell^-})/2$) is shown in Fig. 12(a). The background processes favor emission close to the leptons. For the Higgs signal this closest jet is typically the second quark in the $qq \to qqH$ process and not soft gluon radiation. It is this different angular distribution which is at the heart of the rapidity gap trigger.

A good compromise between strong background rejection and high signal acceptance is achieved by vetoing jets in the veto region defined by

$$p_{\mathrm{T}j}^{\mathbf{veto}} > p_{\mathrm{T},\mathbf{veto}}\,, \qquad \eta_j^{\mathbf{veto}} \varepsilon\, [\eta_\ell^{\mathbf{min}} - 1.7, \eta_j^{\mathbf{tag}}] \text{ or } [\eta_j^{\mathbf{tag}}, \eta_\ell^{\mathbf{max}} + 1.7]\,. \quad (38)$$

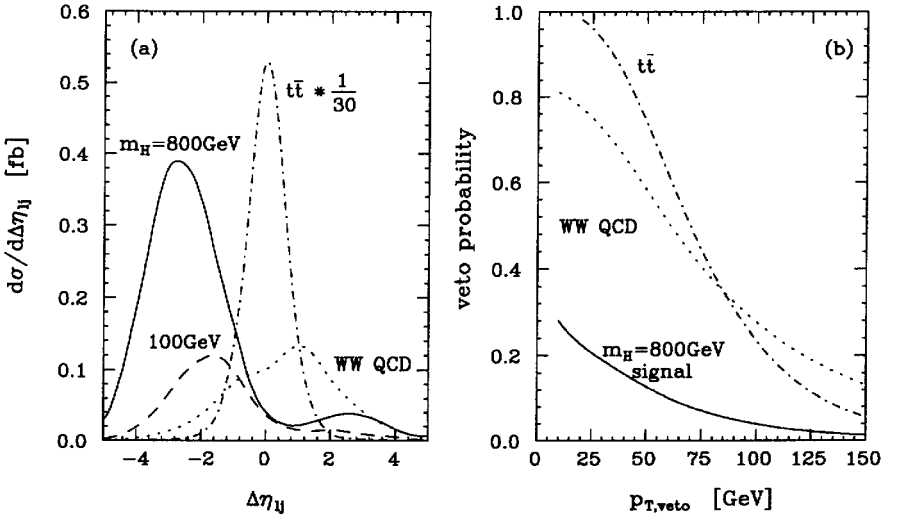

Fig. 12. Rapidity and transverse momentum distributions of secondary jets. In (a) $\Delta\eta_{\ell j}$ measures the pseudorapidity distance of the jet closest to the leptons from the average lepton rapidity $\bar{\eta}$. Negative values of $\Delta\eta_{\ell j}$ correspond to soft jets on the opposite side of the leptons with respect to the tagging-jet. The dashed line shows the distribution for the electroweak background as defined by the $m_H = 100$ GeV case. The $t\bar{t}jj$ background has been scaled down by a factor 30. The probability to find a veto jet candidate above a transverse momentum $p_{T,\text{veto}}$, in the veto region of Eq. (38), is shown in (b). From Ref. [14].

The veto probability as a function of the cut value $p_{\mathbf{T,veto}}$ is shown in Fig. 12(b). Even though these results were obtained in the truncated shower approximation and a more precise modeling is needed, they clearly demonstrate that, in the central region, the backgrounds have a much higher probability to produce additional minijets from QCD radiation than the weak boson scattering signal. Even for the $t\bar{t}$ background, where a strong suppression is obtained by vetoing the central b-quark jets arising from the top decays, the veto on the jet activity from soft QCD radiation provides an additional suppression by a factor 2 for $p_{\mathbf{T,veto}} = 20$ GeV. Final cross section values for signal and backgrounds are given in the last column of Table I. Should minijet vetoing be possible at the LHC for even smaller $p_{\mathbf{T,veto}}$ values then the $t\bar{t}$ background to $H \to WW$ events can effectively be eliminated.

4. Conclusions

Rapidity gaps in hard dijet events at the Tevatron and minijet patterns in weak boson scattering at the LHC have their common origin in processes which are dominated by t-channel color singlet exchange. Both can be understood in terms of soft gluon radiation patterns which are determined by the color structure of the underlying hard scattering event. At the lower energy of the Tevatron the soft gluon radiation pattern is reflected in the distribution of soft hadrons in events without a residual minimum bias event (underlying event). Going up one order of magnitude to LHC energy, "soft gluons" can be hard enough to be seen as distinct minijets, and this opens new strategies for the study of weak boson scattering events.

Via the study of rapidity gap events we are obtaining important information for future LHC physics studies already now at the Tevatron. Similarly, multiple minijet emission, which is expected to be quite common at the LHC, can already now be studied in the hardest "dijet" events at the Tevatron [36, 37]. Both examples show the important interplay between present experiments and new theoretical ideas and tools in multi-parton analysis. Some of these developments were motivated by the search for new physics at future colliders. At the same time they aid in the preparation of experiments at these machines.

Special thanks go to the organizers for making this most enjoyable and stimulating meeting possible. In preparing this talk I have benefitted from many discussions with V. Barger, J. D. Bjorken, A. Brandt, F. Halzen, R. Phillips, and D. Summers and I want to thank them for sharing their insights with me. This research was supported in part by the University of Wisconsin Research Committee with funds granted by the Wisconsin Alumni Research Foundation, and by the U. S. Department of Energy under Grant No. DE-FG02-95ER40896.

REFERENCES

[1] CDF Collaboration, F. Abe *et al.*, *Phys. Rev.* **D50**, 2966 (1994); *Phys. Rev. Lett.* **74**, 2626 (1995); *Phys. Rev.* **D52**, 2605 (1995); D0 Collaboration, S. Abachi *et al.*, *Phys. Rev. Lett.* **74**, 2422 (1995); *Phys. Rev. Lett.* **74**, 2632 (1995); *Phys. Rev.* **D52**, 4877 (1995).

[2] Y.L. Dokshitzer, V.A. Khoze, S. Troyan, in Proceedings of the 6th International Conference on Physics in Collisions, (1986) ed. M. Derrick, World Scientific, Singapore 1987, p.365.

[3] J.F. Gunion *et al.*, *Phys. Rev.* **D40**, 2223 (1989).

[4] J.D. Bjorken, *Int. J. Mod. Phys.* **A7**, 4189 (1992); *Phys. Rev.* **D47**, 101 (1993); preprint SLAC-PUB-5823 (1992).

[5] F.E. Low, *Phys. Rev.* **D12**, 163 (1975); S. Nussinov, *Phys. Rev. Lett.* **34**, 1286 (1975).
[6] D0 Collaboration, S. Abachi *et al.*, *Phys. Rev. Lett.* **72**, 2332 (1994).
[7] CDF Collaboration, F. Abe *et al.*, *Phys. Rev. Lett.* **74**, 855 (1995).
[8] D0 Collaboration, S. Abachi *et al.*, *Phys. Rev. Lett.* **76**, 734 (1996).
[9] For a recent review see *e.g.* J. Bagger *et al.*, *Phys. Rev.* **D49**, 1246 (1994); *Phys. Rev.* **D52**, 3878 (1995).
[10] R.N. Cahn *et al.*, *Phys. Rev.* **D35**, 1626 (1987); V. Barger *et al.*, *Phys. Rev.* **D37**, 2005 (1988); R. Kleiss, W.J. Stirling, *Phys. Lett.* **200B**, 193 (1988).
[11] U. Baur, E.W.N. Glover, *Nucl. Phys.* **B347**, 12 (1990); U. Baur, E.W.N. Glover, *Phys. Lett.* **B252**, 683 (1990); D. Froideveaux, in Proceedings of the ECFA Large Hadron Collider Workshop, Aachen, Germany, 1990, edited by G. Jarlskog and D. Rein CERN report 90-10, Geneva, Switzerland 1990, Vol II, p. 444; M.H. Seymour, in Proceedings of the ECFA Large Hadron Collider Workshop, Aachen, Germany, 1990, edited by G. Jarlskog and D. Rein CERN report 90-10, Geneva, Switzerland 1990, Vol II, p. 557; V. Barger, K. Cheung, T. Han, J. Ohnemus, D. Zeppenfeld, *Phys. Rev.* **D44**, 1426 (1991).
[12] V. Barger, K. Cheung, T. Han, R.J. N. Phillips, *Phys. Rev.* **D42**, 3052 (1990).
[13] V. Barger, K. Cheung, T. Han, D. Zeppenfeld, *Phys. Rev.* **D44**, 2701 (1991); **D48**, 5444E (1993); **D48**, 5433 (1993).
[14] V. Barger, R.J.N. Phillips, D. Zeppenfeld, *Phys. Lett.* **B346**, 106 (1995).
[15] H. Chehime, D. Zeppenfeld, preprint MAD/PH/814 (1994), hep-ph/9401244.
[16] Y.L. Dokshitzer *et al.*, *Rev. Mod. Phys.* **60**, 373 (1988), and references therein.
[17] R.S. Fletcher, T. Stelzer, *Phys. Rev.* **D48**, 5162 (1993).
[18] H. Chehime *et al.*, *Phys. Lett.* **B286**, 397 (1992).
[19] E. Gotsman, E.M. Levin, U. Maor, *Phys. Lett.* **B309**, 199 (1993).
[20] H. Chehime, D. Zeppenfeld, *Phys. Rev.* **D47**, 3898 (1993).
[21] See *e.g.* J.R. Cudell, B.U. Nguyen, *Nucl. Phys.* **B420**, 669 (1994) and references therein.
[22] P.V. Landshoff, O. Nachtmann, *Z. Phys.* **C35**, 405 (1987);
[23] F. Halzen, G.I. Krein, A.A. Natale, *Phys. Rev.* **D47**, 295 (1992); M.B. Gay Ducati, F. Halzen, A.A. Natale, *Phys. Rev.* **D48**, 2324 (1993).
[24] For a more complete discussion see *e.g.* J.F. Gunion, H.E. Haber, G. Kane, S. Dawson, *The Higgs Hunter's Guide*, Addison-Wesley 1990.
[25] J.F. Gunion, A. Stange, S.S.D. Willenbrock, preprint UCD-95-28 (1995), hep-ph/9602238.
[26] D.A. Dicus, R. Vega, *Phys. Rev. Lett.* **57**, 1110 (1986); *Phys. Rev.* **D37**, 2427 (1988); J.F. Gunion, J. Kalinowski, A. Tofighi-Niaki, *Phys. Rev. Lett.* **57**, 2351 (1986); U. Baur, E.W.N. Glover, *Phys. Lett.* **B252**, 683 (1990).
[27] D.A. Dicus, V.S. Mathur, *Phys. Rev.* **D7**, 3111 (1973); B.W. Lee, C. Quigg, H. Thacker, *Phys. Rev.* **D16**, 1519 (1977); M. Veltman, *Acta Phys. Pol.* **B8**, 475 (1977); M.S. Chanowitz, M.K. Gaillard, *Nucl. Phys.* **B261**, 379 (1985).
[28] See *e.g.* V. Barger, R. Phillips, *Collider Physics*, Addison-Wesley 1987.
[29] *Phys. Rev.* **D46**, 2028 (1992).

[30] D. Dicus, J.F. Gunion, R. Vega, *Phys. Lett.* **B258**, 475 (1991); D. Dicus, J.F. Gunion, L.H. Orr, R. Vega, *Nucl. Phys.* **B377**, 31 (1991).
[31] G. Ciapetta, A. DiCiaccio, in Proceedings of the ECFA Large Hadron Collider Workshop, Aachen, Germany, 1990, edited by G. Jarlskog and D. Rein CERN report 90-10, Geneva, Switzerland, 1990, Vol II, p. 155.
[32] A. Duff, D. Zeppenfeld, *Phys. Rev.* **D50**, 3204 (1994).
[33] A. Stange, private communication.
[34] V. Barger, T. Han, J. Ohnemus, D. Zeppenfeld, *Phys. Rev.* **D41**, 2782 (1989).
[35] V. Barger, R.J.N. Phillips, *Phys. Rev. Lett.* **55**, 2752 (1985); H. Baer, V. Barger, H. Goldberg, R.J.N. Phillips, *Phys. Rev.* **D37**, 3152 (1988).
[36] CDF Collaboration, F. Abe *et al.*, *Phys. Rev. Lett.* **75**, 608 (1995).
[37] D. Summers, D. Zeppenfeld, preprint MADPH-95-904 (1995), hep-ph/9509206.